

Fragile Glasses Associated with a Dramatic Drop of Entropy under Supercooling

Chun-Shing Lee¹, Matteo Lulli^{1,2}, Ling-Han Zhang³, Hai-Yao Deng⁴, and Chi-Hang Lam^{1*}

¹*Department of Applied Physics, Hong Kong Polytechnic University, Hong Kong, China*

²*Department of Mechanics and Aerospace Engineering,*

Southern University of Science and Technology, Shenzhen, Guangdong 518055, China

³*Department of Physics, Carnegie Mellon University, Pittsburgh, Pennsylvania 15213, USA*

⁴*School of Physics and Astronomy, Cardiff University,*

5 The Parade, Cardiff CF24 3AA, Wales, United Kingdom

(Dated: December 22, 2020)

We perform kinetic Monte Carlo simulations of a distinguishable-particle lattice model of structural glasses with random particle interactions. By varying the interaction distribution and the average particle hopping energy barrier, we obtain an extraordinarily wide range of kinetic fragility. A stretching exponent, characterizing structural relaxation, is found to decrease with the kinetic fragility in agreement with experiments. The most fragile glasses are those exhibiting low hopping barriers and, more importantly, dramatic drops of entropies upon cooling toward the glass transition temperatures. The entropy drops reduce possible kinetic pathways and lead to dramatic slowdowns in the dynamics. In addition, the kinetic fragility is shown to correlate with a thermodynamic fragility.

An important concept in the study of structural glasses [1–3] is the kinetic fragility, often simply called the glass fragility, which has been investigated in great detail for different types of glass formers [4–7]. It describes how rapidly the dynamics slows down when temperature decreases. The dynamics is typically characterized by viscosity, structural relaxation time [8, 9], or particle diffusion coefficient [10, 11]. Glasses possessing the most dramatic slowdown are classified as fragile, whereas the opposite are referred to as strong. Several models of glasses have been able to reproduce a range of kinetic fragilities [12–16]. A closely related thermodynamic fragility [17] has also been defined and is based on how dramatically the entropy drops as the temperature decreases. Experimental results indicate, in general, a positive correlation between the kinetic and thermodynamic fragilities [17, 18]. Yet, a fundamental understanding of the fragilities and their relationship is still lacking.

In this Letter, we study the kinetic and thermodynamic fragilities using a recently proposed distinguishable particle lattice model (DPLM) of structural glasses [19]. Lattice models are instrumental in statistical physics. Celebrated examples include the Ising model for magnetism and the Edwards-Anderson model for spin glasses [20]. By bridging between analytic theory and more realistic models, they play pivotal roles in the solution and intuitive understanding of the systems concerned. The DPLM aims at this bridging task for the study of structural glass. It possesses exactly solvable equilibrium statistics [19] and is promising for analytical treatment [21, 22]. In support of its validity as a model of glass, DPLM has successfully reproduced typical glassy behaviors [19], a remarkable phenomenon known as Kovacs’ expansion gap paradox [23], as well as Kovacs’ effect for the aging of glasses [24]. It captures in simpler and

more tractable form the relevant physics seen in molecular dynamics (MD) and other realistic models, which in turn are more detailed approximate models of glasses. This should be a worthwhile approach considering that direct analytical treatment of MD or experimental systems in finite dimensions has proved exceedingly challenging and controversial [3].

Here, we show that both the kinetic and thermodynamic fragilities of the DPLM can be varied over wide ranges of values via the fine-tuning of its kinetic and thermodynamic properties. Modeled glasses with higher kinetic fragilities in general exhibit smaller stretching exponents as well as higher thermodynamic fragilities, in good qualitative agreement with experiments. The fundamental mechanisms behind the fragility variations in this model are intuitively understandable, and are likely applicable also to realistic glasses [22].

We adopt the DPLM proposed in Ref. [19], with minor differences explained in Sec. I in supplementary information (SI). It is defined on a 2D square lattice of size L^2 with $L = 100$ and unit lattice constant following periodic boundary conditions. There are N distinguishable particles on the lattice labeled from 1 to N . Each lattice site i can be occupied by at most one of the particles with a particle index $s_i = 1, 2, \dots, N$. For unoccupied sites, i.e., sites occupied by voids, $s_i = 0$. A void density of $\phi_v = 0.01$ is considered. A particle configuration is specified by the set of particle indices $\{s_i\}$ over all sites. The total energy is

$$E = \sum_{\langle i,j \rangle'} V_{s_i s_j}, \quad (1)$$

where the sum is restricted to nearest neighbor (NN) sites i and j occupied by particles. The interaction V_{kl} for each pair of adjacent particles k and l is sampled before the start of the simulation from the pair-interaction distribution $g(V_{kl})$ and fixed subsequently. The particle index s_i is time dependent since the site i will be visited by

* Email: C.H.Lam@polyu.edu.hk

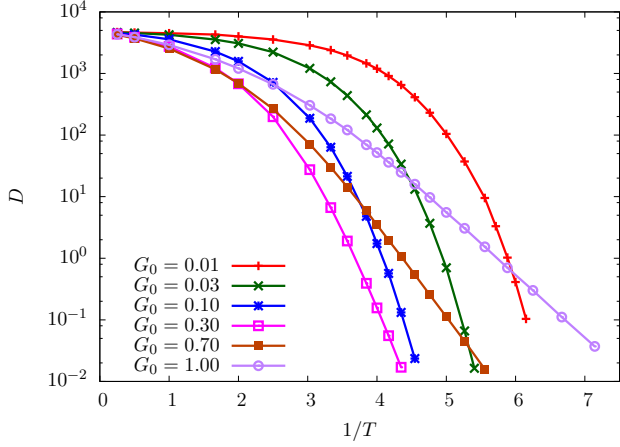


Figure 1. Arrhenius plot of D for various G_0 at $E_0 = 0$. The system with a lower G_0 is more super-Arrhenius.

different particles as the system evolves. Thus, $V_{s_i s_j}$ in Eq. (1) is time dependent, although any V_{kl} for any given particles k and l is quenched. Dimensionless units will be adopted.

Particle distinguishability and particle-dependent interactions are directly justifiable for polydisperse or polymer systems. For identical-particle systems, it instead accounts effectively for the generally different frustration states experienced by the particles. It also models high-entropy alloys [25] in the limit of a large number of atomic species. Being a lattice model, particle vibrations are not explicitly accounted for. A particle configuration more precisely models an inherent state of a realistic system [22].

A main feature of our work is the random sampling for each $V_{kl} \in [V_0, V_1] \equiv [-0.5, 0.5]$ from a *bicomponent distribution* consisting of a uniform and a delta function representing, respectively, unexcited and excited states given by

$$g(V) = \frac{G_0}{\Delta V} + (1 - G_0)\delta(V - V_1), \quad (2)$$

where $\Delta V = V_1 - V_0 = 1$ and δ denotes the Dirac delta function. Here, $G_0 \in [0, 1]$ is our main thermodynamic parameter controlling the fragilities. It equals the probabilistic weight of the uniform unexcited component of the distribution and also the probability density $g(V_0)$ at the ground state energy V_0 . For $G_0 = 1$, Eq. (2) reduces to the uniform distribution adopted in Ref. [19], which leads to a strong glass. Alternatively, for $G_0 = 0$, all interactions are at the excited energy state V_1 and the model reduces to a simple identical-particle lattice gas with a uniform particle interaction.

We assume a void-induced dynamics, which has been directly observed in recent experiments on glassy colloidal systems [26]. Using the Metropolis algorithm, each particle can hop to an unoccupied NN site at temperature

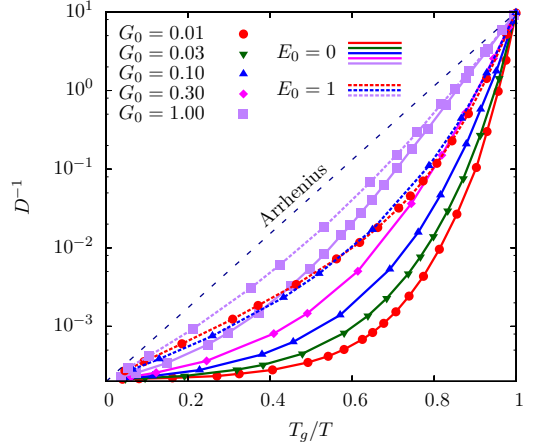


Figure 2. Kinetic Angell plot of D^{-1} against T_g/T for various G_0 and E_0 , where T_g for each curve is defined at $D_r = 10^{-1}$. A low G_0 gives a fragile system. For a given G_0 , increasing E_0 makes the system stronger.

T at a rate

$$w = \begin{cases} w_0 \exp[-(E_0 + \Delta E)/k_B T] & \text{for } \Delta E > 0, \\ w_0 \exp(-E_0/k_B T) & \text{for } \Delta E \leq 0, \end{cases} \quad (3)$$

where ΔE is the change in the system energy E given by Eq. (1) due to the hop and $k_B = 1$ is the Boltzmann constant. We put $w_0 = 10^6$. The hopping energy barrier offset $E_0 \geq 0$ is our main kinetic model parameter for controlling the fragilities. Our algorithm satisfies detailed balance.

Kinetic Monte Carlo simulations have been performed on the DPLM, starting from directly constructed initial equilibrium configurations [19]. We report here our main results while further details are given in Sec. II in SI. The particle mean squared displacement defined as $\text{MSD} = \langle |\mathbf{r}_l(t) - \mathbf{r}_l(0)|^2 \rangle$ is calculated, where $\mathbf{r}_l(t)$ denotes the position of particle l at time t . The particle diffusion coefficient D is computed according to $D = (1/2d) (\text{MSD}/t)$, where $d = 2$ is the dimension of the system, at sufficiently large values of t in the diffusion regime.

The Arrhenius plot in Fig. 1 shows D against $1/T$ for $E_0 = 0$ and various G_0 . We observe that $\log D$ decreases with $1/T$ faster than linearly, demonstrating a super-Arrhenius slowdown. The dependence of D on G_0 for any given T is nonmonotonic. Yet, the super-Arrhenius behavior strengthens monotonically as G_0 decreases. This can be clearly seen in a *kinetic Angell* plot in Fig. 2, which plots D^{-1} against T_g/T for $E_0 = 0$ (solid lines) using the data from Fig. 1. We have defined the glass transition temperature T_g as T at which $D = D_r \equiv 10^{-1}$, where the reference diffusion coefficient D_r is about the lowest value we can simulate. We observe that D now varies monotonically with G_0 for any given T_g/T . More importantly, the super-Arrhenius property clearly strengthens monotonically as G_0 decreases. Related kinetic Angell

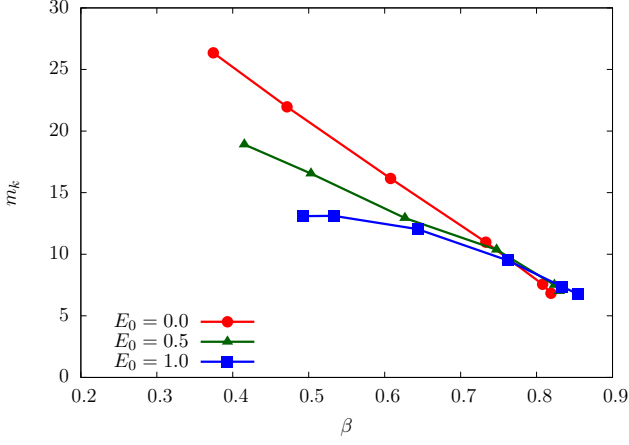


Figure 3. Relationship between m_k and β at $E_0 = 0, 0.5, 1$ with $G_0 = 0.01, 0.03, 0.1, 0.3, 0.7, 1$ (from left to right).

plot of structural relaxation time extracted from self-intermediate scattering function shows closely analogous trends (see Sec. II in SI).

Figure 2 also shows D^{-1} for $E_0 = 1$ (dotted lines). Results are simply obtained from values of D for $E_0 = 0$ after rescaling time by a factor $\exp(E_0/k_B T)$, noting that T_g has to be recalculated since D_r is not rescaled. We observe that a smaller E_0 strengthens the super-Arrhenius property at any given G_0 . The results in Fig. 2 capture many qualitative features in experimental findings [5–7].

The kinetic fragility m_k describes the super-Arrhenius property quantitatively and is defined by $m_k = \partial \log D^{-1} / \partial (T_g/T) |_{T=T_g}$. We obtain a wide range of values of m_k from 6.76 to 26.35. These values are in general smaller than experimental ones typically in the range from 25 to 150 [27], but this is only due to a rather small D_r adopted for defining T_g . An extrapolation to $D_r = 10^{-14}$ is performed so that nearly 18 orders of magnitude of D are considered, similar to analyses of structural relaxation time and viscosity in experiments [8, 9]. Then, m_k ranges from 21.4 for large G_0 and E_0 and 120 for $G_0 = 0.01$ and $E_0 = 0$, consistent with the experimental range (see Sec. III in SI).

To further establish the physical relevance of the DPLM, we proceed to show that relaxation and thermodynamic properties of the strong and fragile glasses from this model are consistent with experiments. First, structural relaxation is studied by measuring the self-intermediate scattering function

$$F_s(\mathbf{q}, t) = \left\langle e^{i\mathbf{q} \cdot (\mathbf{r}_l(t) - \mathbf{r}_l(0))} \right\rangle, \quad (4)$$

where $q = (2\pi/L)q'$ with $q' = 10$. The results are nicely fitted by the stretched exponential function $A \exp[-(t/\tau)^\beta]$ for $t \gtrsim \tau$, where β , τ , and A are, respectively, the stretching exponent, the relaxation time, and a constant close to unity. Figure 3 plots m_k against β at T_g for various G_0 and E_0 . It shows that m_k tends to decrease approximately linearly with β , in agreement with

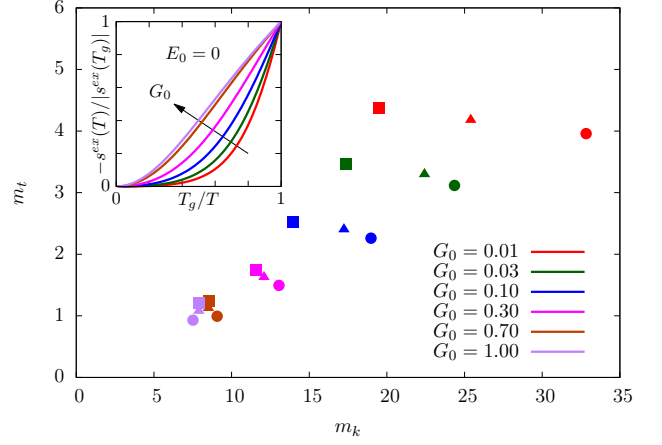


Figure 4. Plot of m_t against m_k at $E_0 = 0$ (circle), 0.5 (triangle), and 1 (square) for various G_0 . Inset: Thermodynamic Angell plot of $-s^{\text{ex}}(T)/|s^{\text{ex}}(T_g)|$ at $E_0 = 0$.

a trend observed previously in experiments [27]. In addition, the obtained range 0.37 to 0.81 of β is comparable to that from experiments. Results on β are not significantly affected by using smaller values of D_r , especially for the fragile glasses since T_g only changes slightly.

Second, we study the thermodynamic properties of our model by calculating an entropy-based *thermodynamic fragility*. The equilibrium statistics including the partition function Z of the DPLM are exactly known [19]. The entropy per particle $s(T)$ is computed accordingly. We further define an excess entropy per particle $s^{\text{ex}}(T) = s(T) - s^{\text{LG}}$ over the entropy s^{LG} of a simple lattice gas [28]. [See Eq. (S23).] The inset of Fig. 4 shows a *thermodynamic* Angell plot of $-s^{\text{ex}}(T)/|s^{\text{ex}}(T_g)|$ against T_g/T for $E_0 = 0$ and different G_0 . The results resemble those of closely related thermodynamic Angell plots from experiments [29] as well as the kinetic Angell plot in Fig. 2. An increased E_0 alters the curvature only slightly for all values of G_0 . In general, a strong glass with $G_0 = 1$ is also thermodynamically strong with a close-to-linear relation, while a fragile glass at $G_0 = 0.01$ shows the most dramatic variations. The trend is in general similar if other forms of thermodynamic Angell plots [29] are considered.

We define a thermodynamic fragility m_t as

$$m_t = \left. \frac{\partial (-s^{\text{ex}}(T)/|s^{\text{ex}}(T_g)|)}{\partial (T_g/T)} \right|_{T=T_g}, \quad (5)$$

which is analogous to the kinetic counterpart m_k . Figure 4 shows the kinetic fragility m_t against the thermodynamic fragility m_k for various G_0 and E_0 , displaying a clear tendency of a positive correlation, i.e., $m_t \sim m_k$. The correlation is consistent with the general trend observed in experiments based on related definitions [29] and is mainly caused by the similar dependencies of m_k and m_t on G_0 .

We have studied glass fragility using the DPLM for

various values of model parameters G_0 and E_0 . The most fragile glass is obtained at small G_0 and $E_0 = 0$. Extrapolating our simulation results toward $G_0 \rightarrow 0$, the kinetic fragility m_k appears to rise unboundedly (see Fig. S12). The DPLM may hence model in-principle arbitrarily fragile glasses. Simulations at very small G_0 are, however, prohibitively intensive due to increased finite-size effects. At $G_0 = 0$, the model reduces to a simple lattice gas, which is not glassy. A high m_k thus requires a small but nonvanishing probability of low-energy particle pairings.

We argue that G_0 is the main material parameter which captures the relevant particle interaction characteristics and determines the fragilities m_t and m_k in glasses. The value of G_0 in a glass depends on the detailed molecular interactions and is strongly affected, for example, by the geometries of any tightly bounded groups of atoms. A fragile glass obtained at a small G_0 can be intuitively understood as follows. At high T , all particle configurations are possible, leading to a high entropy $s(T)$ independent of G_0 . Most interactions take the excited states with energy V_1 due to their high probabilistic weight $1 - G_0$ [see Eq. (2)]. Particle pairings with unexcited energies close to V_0 are in contrast rare due to the small probabilistic weight G_0 . As T decreases, the lower energies render them energetically favorable and increasingly dominant. The entropy $s(T)$ thus drops dramatically and becomes small at low T , accounting for a high m_t .

We further suggest that this high m_t is closely correlated to a high m_k . This is because the system dynamics at low T amounts to sampling various energetically favorable configurations. The rarity of these configurations as indicated by the low entropy implies highly constrained kinetic pathways of particle motions. This leads to a sharp drop in D as described by a large m_k . A possible characteristic of constrained kinetics is repetitive particle motions. Our picture is thus supported by a sharp increase in a particle return probability but a mild drop of the particle hopping rate as T decreases as explained in Sec. II in SI. The thermodynamic parameter G_0 therefore strongly impacts the system thermodynamics and hence also the kinetics. In contrast, the kinetic parameter E_0 is of lesser importance to the fragility properties. By controlling the hopping barrier, it clearly has a strong and direct impact on m_k . However, it plays no role in the equilibrium statistics and in particular in the system entropy [see Eq. (S23)]. It has a tiny impact on m_t only by influencing the value of T_g at which m_t is evaluated. Not accounting for the correlation between m_k and m_t observed in experiments, we expect E_0 to play a smaller role in the variation of m_k among various glasses.

The particle interaction distribution $g(V)$ has been taken with a bicomponent form consisting of a low-energy uniform distribution and a high-energy delta function for simplicity. The delta function represents excited particle interactions more relevant at higher T and replacing it by some narrow Gaussian leads to similar simulation results.

The uniform distribution is the simplest continuous distribution with a lower bound V_0 , corresponding to the energy minimum present in typical pair potentials such as the Lennard-Jones potential. The continuous form of $g(V)$ around V_0 is expected to lead to glassy behaviors even at a very low T , as the model reduces to one with a single uniform distribution studied in Ref. [19].

The DPLM with a bicomponent $g(V)$ is closely related to a bond excitation model proposed by Moynihan and Angell [30], in which particle bonds can assume either an unexcited or excited state (see Sec. VI in SI). At low T , the realized interactions $V_{s_i s_j}$ from the uniform unexcited component have a small energy spread of about $k_B T$ around $V_0 + k_B T$. Neglecting this energy spread, the ratio of the degeneracy of the excited states to that of the unexcited states is about $(1 - G_0)/G_0$, leading to an entropy difference

$$\Delta S^0 \simeq k_B \ln[(1 - G_0)/G_0]. \quad (6)$$

Considering $G_0 = 0.01$ corresponding to fragile glasses, we get $\Delta S^0 \simeq 4.60 k_B$. A more accurate calculation using Eq. (S45) gives a similar value of $\Delta S^0 \simeq 5.42 k_B$. Reverting to physical units with $k_B = 8.315$ J/mol K, it gives $\Delta S^0 \simeq 45.1$ J/K per mole of excitable states. This value matches that of ΔS^0 , for example, for toluene in Ref. [30], which has a high $m_k = 103$. In addition, $\Delta H^0 \simeq 1 - k_B T_g$ is the energy difference between the excited and unexcited states in our model. At $T_g \simeq 0.163$, $\Delta H^0/k_B T_g \simeq (1 - 0.163)/0.163 \simeq 5.15$ for $G_0 = 0.01$. It compares well with the value 6.95 for toluene in Ref. [30].

The quantitative consistency demonstrated above means that the bond excitation model provides a simplified theoretical description for the thermodynamic properties of the DPLM with the bicomponent $g(V)$. Moreover, the success of the bond excitation model in describing the entropy of fragile glasses in Ref. [30] justifies the bicomponent form of $g(V)$ used in this work. From Eq. (6), a fragile glass characterized by a small G_0 possesses a large ΔS^0 . These material parameters depend on the detailed molecular interactions. For molecular or polymer glasses which are often fragile, their values may reflect that the geometrically complex molecules fit well with each other to form very stable bonds only at a rare set of orientations and conformations. In contrast, strong glasses including network glasses may consist of simpler structures such as tetrahedrons. A simple random spread of the interactions due to frustration can then account for $G_0 \simeq 1$ and a small ΔS^0 .

We have found that the thermodynamic parameter G_0 has the strongest impacts on both m_k and m_t . In contrast, the kinetic parameter E_0 also plays a significant role for m_k but not so much for m_t . Further simulations show that the void density ϕ_v has rather small effects on both m_k and m_t , as long as $\phi_v \ll 1$ which ensures the glassy state. One can also consider model variations such as a different $g(V)$. Since glass properties depend on multiple model parameters, the relations discussed here between m_k , m_t , and β are only general trends assuming

small variations in other parameters. Exceptions are thus possible in more general settings. From another point of view, the value of m_k does not uniquely determine the precise geometry of the whole curve in the Angell plot in Fig. 2 when multiple material parameters are taken into account. These are fully consistent with experimental observations [5].

To sum up, we have studied fragility properties of glasses using kinetic Monte Carlo simulations and analytic calculations based on the DPLM. A wide range of values of kinetic fragility is reproduced, indicating the possibility of arbitrarily fragile glasses limited only by computational resources. The kinetic fragility is mainly controlled via a thermodynamic parameter G_0 , dictating the probability distribution of particle pair interactions. The most fragile glass is obtained at small G_0 corresponding to the case that pair interactions can take low-energy states with a small but nonvanishing probability, i.e. low-entropy unexcited states. These configurations physically represent rare pairings between particles with exception-

ally stable arrangements. As the temperature decreases, particle configurations are increasingly constrained to these low-energy pairings. This causes a dramatic drop in the entropy associated with a dramatic slowdown in the dynamics, resulting, respectively, in high thermodynamic and kinetic fragilities. Our model, upon variations in G_0 , exhibits correlations between kinetic fragility, thermodynamic fragility, and a relaxation stretching exponent, in qualitative agreement with general trends observed in experiments. The kinetic fragility is also affected by a kinetic model parameter E_0 . A fragile glass is obtained at small E_0 corresponding to particle hopping activation barriers with an average which is small compared to their fluctuations.

We thank the support of Hong Kong GRF (Grant No. 15330516), Hong Kong PolyU (Grant No. 1-ZVGH), and National Natural Science Foundation of China (Grant No. 11974297).

-
- [1] L. Berthier and G. Biroli, “Theoretical perspective on the glass transition and amorphous materials,” *Rev. Mod. Phys.* **83**, 587 (2011).
 - [2] J. P. Garrahan, P. Sollich, and C. Toninelli, “Kinetically constrained models,” in *Dynamical Heterogeneities in Glasses, Colloids and Granular Media*, edited by L. Berthier, G. Biroli, J.-P. Bouchaud, L. Cipelletti, and W. van Saarloos (Oxford University Press, 2011).
 - [3] F. H. Stillinger and P. G. Debenedetti, “Glass transition thermodynamics and kinetics,” *Annu. Rev. Condens. Matter Phys.* **4**, 263 (2013).
 - [4] R. Bohmer, K. L. Ngai, C. A. Angell, and D. J. Plazek, “Nonexponential relaxations in strong and fragile glass formers,” *J. Chem. Phys.* **99**, 4201 (1993).
 - [5] C. A. Angell, “Formation of glasses from liquids and biopolymers,” *Science* **267**, 1924 (1995).
 - [6] L.-M. Wang, C. Austen Angell, and R. Richert, “Fragility and thermodynamics in nonpolymeric glass-forming liquids,” *J. Chem. Phys.* **125**, 074505 (2006).
 - [7] Daniele Giordano and Donald B. Dingwell, “The kinetic fragility of natural silicate melts,” *Journal of Physics: Condensed Matter* **15**, S945–S954 (2003).
 - [8] C. A. Angell, “Relaxation in liquids, polymers and plastic crystals — strong/fragile patterns and problems,” *J. Non-Cryst. Solids* **131-133**, 13 (1991).
 - [9] C. Alba, L. E. Busse, D. J. List, and C. A. Angell, “Thermodynamic aspects of the vitrification of toluene, and xylene isomers, and the fragility of liquid hydrocarbons,” *J. Chem. Phys.* **92**, 617 (1990).
 - [10] F. Fujara, B. Geil, H. Sillescu, and G. Fleischer, “Translational and rotational diffusion in supercooled orthoterphenyl close to the glass transition,” *Z. Phys. B* **88**, 195 (1992).
 - [11] D. Coslovich and G. Pastore, “Understanding fragility in supercooled lennard-jones mixtures. i. locally preferred structures,” *J. Chem. Phys.* **127**, 124504 (2007).
 - [12] J. P. Garrahan and D. Chandler, “Geometrical explanation and scaling of dynamical heterogeneities in glass forming systems,” *Phys. Rev. Lett.* **89**, 035704 (2002).
 - [13] F. Sausset, G. Tarjus, and P. Viot, “Tuning the fragility of a glass-forming liquid by curving space,” *Phys. Rev. Lett.* **101**, 155701 (2008).
 - [14] A. Parmar and S. Sastry, “Kinetic and thermodynamic fragilities of square well fluids with tunable barriers to bond breaking,” *J. Phys. Chem. B* **119**, 11243 (2015).
 - [15] O. Misaki, K. Kang, and M. Kunimasa, “Tuning pairwise potential can control the fragility of glass-forming liquids: from a tetrahedral network to isotropic soft sphere models,” *J. Stat. Mech.* **2016**, 074002 (2016).
 - [16] S. Ciarella, R. A. Biezemans, and L. Janssen, “Understanding, predicting, and tuning the fragility of vitrimeric polymers,” arXiv:1910.00468 (2019).
 - [17] C. A. Angell and K. Ueno, “Soft is strong,” *Nature* **462**, 45 (2009).
 - [18] F. Giulia, D. and B. Livio, “Thermodynamic and dynamic fragility in metallic glass-formers,” *Acta Materialia* **61**, 2260 (2013).
 - [19] L.-H. Zhang and C.-H. Lam, “Emergent facilitation behavior in a distinguishable-particle lattice model of glass,” *Phys. Rev. B* **95**, 184202 (2017).
 - [20] S. F. Edwards and P. W. Anderson, “Theory of spin glasses,” *Journal of Physics F: Metal Physics* **5**, 965 (1975).
 - [21] C.-H. Lam, “Local random configuration-tree theory for string repetition and facilitated dynamics of glass,” *J. Stat. Mech.* **2018**, 023301 (2018).
 - [22] H.-Y. Deng, C.-S. Lee, M. Lulli, L.-H. Zhang, and C.-H. Lam, “Configuration-tree theoretical calculation of the mean-squared displacement of particles in glass formers,” *J. Stat. Mech.* **2019**, 094014 (2019).
 - [23] M. Lulli, C. S. Lee, H. Y. Deng, C. T. Yip, and C. H. Lam, “Spatial Heterogeneities in Structural Temperature Cause Kovacs’ Expansion Gap Paradox in Aging of Glasses,” *Phys. Rev. Lett.* (2020), 10.1103/Phys-

- [RevLett.124.095501](#).
- [24] M. Lulli, L.-H. Zhang, C.-S. Lee, H.-Y. Deng, and C.-H. Lam, [arXiv:1910.10374](#) (2019).
 - [25] J.-W. Yeh, “Alloy design strategies and future trends in high-entropy alloys,” [JOM](#) **65**, 1759 (2013).
 - [26] Cho-Tung Yip, Masaharu Isobe, Chor-Hoi Chan, Simiao Ren, Kin-Ping Wong, Qingxiao Huo, Chun-Sing Lee, Yuen-Hong Tsang, Yilong Han, and Chi-Hang Lam, “Direct evidence of void induced structural relaxations in colloidal glass formers,” (2020), [arXiv:2011.02754 \[cond-mat.soft\]](#).
 - [27] M. Matthieu, “Relaxation and physical aging in network glasses: a review,” [Rep. Prog. Phys.](#) **79**, 066504 (2016).
 - [28] J. C. Dyre, “Perspective: Excess-entropy scaling,” [J. Chem. Phys.](#) **149**, 210901 (2018).
 - [29] L. M. Martinez and C. A. Angell, “A thermodynamic connection to the fragility of glass-forming liquids,” [Nature](#) **410**, 663 (2001).
 - [30] C. T. Moynihan and C. A. Angell, “Bond lattice or excitation model analysis of the configurational entropy of molecular liquids,” [J. Non-Cryst. Solids](#) **274**, 131 (2000).

Supplementary Information for Fragile Glasses Associated with a Dramatic Drop of Entropy under Supercooling

I. MODEL DETAILS: DIFFERENCES FROM PREVIOUS DEFINITION

We now provide further details of the DPLM adopted in this work, focusing on the differences of this variant with respect to that in Ref. [1]. A main feature in this work is to study a bicomponent form of the pair-interaction energy distribution $g(V)$, generalizing a simple uniform distribution used in Ref. [1]. This has been discussed in the main text. Here, we explain other differences.

Particle-dependent interactions: In this work, we consider a particle-dependent interaction V_{kl} between nearest neighboring (NN) particles, which depends only on the particle labels k and l (see Eq. (1) of the main text). This is a simplification from Ref. [1] which uses a site-particle-dependent interaction V_{ijkl} with additional explicit dependences on the sites i and j at which particles k and l are located. In Ref. [1], the explicit site dependence was introduced to model different frustration states at different sites. It was already shown analytically in Ref. [1] that the same exact equilibrium statistics hold for both V_{ijkl} and V_{kl} types of interactions. We have verified that adopting either V_{ijkl} or V_{kl} gives qualitatively similar features for all numerical measurements reported in Ref. [1] and in this work. Only minor quantitative differences are observed in general.

Although both V_{ijkl} and V_{kl} interaction types should in principle be applicable in this work, the computation for the case of V_{ijkl} is more intensive and is thus not adopted. Specifically, the whole set of V_{ijkl} requires a memory allocation of size $\sim N^3 \sim L^6$, for the case of N particles in a nearly fully occupied lattice of linear size L . Using a two-step interaction energy tabulation approximation, the requirement reduces to a manageable size of $\sim N^2$. This approximation has been verified to be accurate for $G_0 = 1$ in particular by checking that the system energy E [see Eq. (1)] measured from simulations agrees with an exact theoretical value [1]. However, we find in this work that the accuracy can deteriorate as G_0 decreases because the approximation admits strong finite size effects. For example, for $G_0 = 0.01$, $L = 100$ and $T = 0.22$, the measured E deviates by about 18% from the theoretical value. The error reduces if a larger L is used, but memory requirements may then be too demanding. In contrast, using V_{kl} for the same conditions, the discrepancy in E decreases to only about 0.6%. The memory consumption to store the whole set of V_{kl} is also of a manageable size of $\sim N^2$ without needing the two-step interaction energy tabulation approximation.

Metropolis algorithm: We apply a Metropolis form of

the particle hopping rate w in Eq. (3) with a hopping energy barrier $E_0 + \max\{\Delta E, 0\}$, where ΔE is the change of the system energy E induced by the hop attempt and E_0 is an energy barrier offset. The energy barrier must be non-negative in all cases and this requires $E_0 \geq 0$. In Ref. [1], an activated-hopping form of the rate was used instead. A similar enforcement of the non-negativity of the energy barriers leads to a constraint $E_0 \geq 1.5$ for an analogously defined offset E_0 . Both the Metropolis and the activated hopping algorithms are widely used dynamics in simplified forms and both satisfy detailed balance. Nevertheless, an offset of $E_0 = 0$ is only possible for the Metropolis algorithm and it corresponds to the case of a small average barrier or equivalently large barrier fluctuations. We have found in this work that this is the regime in which the most fragile glass can be obtained. In addition, dynamical pathways with the minimum possible barriers consistent with detailed balance in general exist according to potential energy landscape calculations on amorphous silica [2]. The Metropolis form is thus adopted to realize a wider range of fragilities. Interestingly, our results suggest that very fragile glasses have large fluctuations in the particle hopping energy barriers, which may be more consistent with the Metropolis function than the activated hopping function.

II. DETAILED SIMULATION RESULTS

Diffusion coefficient and Mean square displacement: Figure S1 shows our kinetic Monte Carlo simulation results on the mean square displacement $\text{MSD}(t)$ versus t for the example of a fragile glass at $G_0 = 0.01$ and $E_0 = 0$. At each temperature T , we extract the diffusion coefficient D from $D = (1/2d) (\text{MSD}/t)$ with $d = 2$ at sufficiently large t in the diffusive regime. Specifically, we require that t is large enough to ensure that $\text{MSD} > 1$ and $\text{MSD} \propto t^\gamma$ with $0.95 \leq \gamma \leq 1$. For other values of G_0 , the MSD is similarly measured and all results on D are shown in Fig. 1 in the main text.

As observed in Fig. 1, the dependence of D on G_0 for any given T is nonmonotonic. This can be explained as follows. The energy E of the system equals the sum of all realized pair interactions $V_{s_i s_j}$ [See Eq. (1)]. D is smallest when particle hops involve the maximum fluctuations in $V_{s_i s_j}$. This is because excitations from the very stable states slow down the dynamics. Take $T = 0.25$ as an example. When G_0 is small, nearly all $V_{s_i s_j}$ equal $V_1 = 0.5$ and this results in a high D in Fig. 1. When $G_0 = 1$, $V_{s_i s_j}$ are distributed mainly in the range $(V_0 + k_B T) \pm k_B T$ with $V_0 = -0.5$ and $k_B = 1$, which is still a narrow range. This hence also leads to a relatively high D . In contrast,

for $G_0 \sim 0.3$, $V_{s_i s_j}$ jumps between $(V_0 + k_B T)$ and V_1 , as neither component of the interactions are negligible. This results in large fluctuations in the energies of the configurations related by particle hops and hence a small D . The precise minimized point of D depends also on entropic effects and thus on T .

From Fig. S1, we observe the emergence of a plateau characteristic of glasses as T decreases. The MSD for the example of a strong glass has been shown in Ref. [1]. Compared with a strong glass, results on the fragile glass in Fig. S1 exhibits a much more stretched-out plateau at low T . Despite the shallow plateaus in the MSD shown in Fig. S1 and in Ref. [1], our systems at low T is in fact deeply supercooled, by common measures in typical lattice or molecular dynamics (MD) simulations. Due to the lack of lattice vibrations, lattice simulations even in deeply supercooled regime always show shallow plateaus (see e.g. [3]). The MSD in Fig. S1 more precisely represents MSD of coarse-grained particle positions. It can be compared directly with the MSD based on the evolution of particle positions in inherent structures [4], which have been demonstrated computationally to possess a much shallower plateau than those with vibrations [5]. If one would add to the MSD the contribution of vibrations using some adiabatic approach, the plateau will be located around $\text{MSD} \simeq 0.1$, a typical value for particles of unit size. The plateau will then become much broader and more pronounced.

We have performed independent simulations for different values of T and G_0 primarily for $E_0 = 0$ as discussed above. Results for other values of $E_0 > 0$ can be trivially obtained from those at $E_0 = 0$ by rescaling time by a factor $\exp(E_0/k_B T)$, without performing further simulations. The diffusion coefficient D at $E_0 > 0$ is simply obtained by multiplying the corresponding value of D for $E_0 = 0$ by a factor $\exp(-E_0/k_B T)$. Note that we define T_g as T at which $D = D_r \equiv 0.1$, where the reference D_r remains a constant admitting no rescaling. As D is rescaled, T_g is varied and is recalculated from $D = D_r$. Results on D and T_g accordingly calculated for various E_0 are applied in Fig. 2 in the main text.

Temperature dependent void density: Simulations in the main text are done with a fixed void density $\phi_v = 0.01$ for simplicity, which is a small value more appropriate for glasses at low T with limited free volumes. In reality, ϕ_v should increase as T increases. To model this phenomenon, we perform further simulations at $G_0 = 0.1$ and $E_0 = 0$ assuming a T dependent ϕ_v given by

$$\phi_v(T) = \phi_v^\infty e^{-E_v/k_B T}, \quad (\text{S1})$$

where ϕ_v^∞ denotes the void density at the high T limit and E_v is the free energy cost of void formation. We take $\phi_v^\infty = 0.30$ and $E_v = 0.75$. At high T , $\phi_v \simeq \phi_v^\infty$ so that voids are abundant and particles can diffuse relatively freely as expected in non-glassy liquids. At low T , the model crosses over to the case with $\phi_v = 0.01$, noting

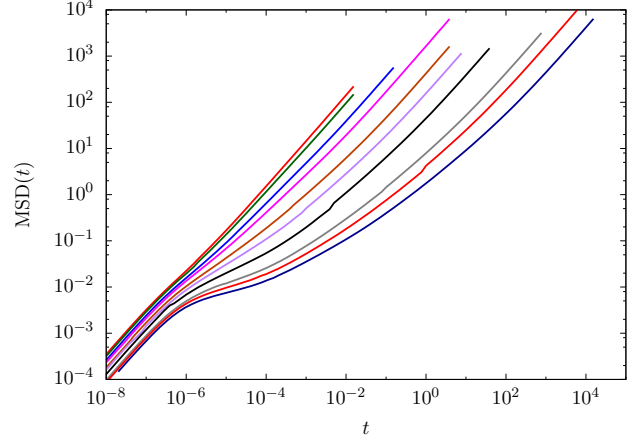


Figure S1. $\text{MSD}(t)$ against t at $G_0 = 0.01$ and $E_0 = 0$. Different curves represent different $T = 0.4, 0.3, 0.24, 0.22, 0.2, 0.19, 0.18, 0.175, 0.17, 0.1667, 0.1626$ (from left to right).

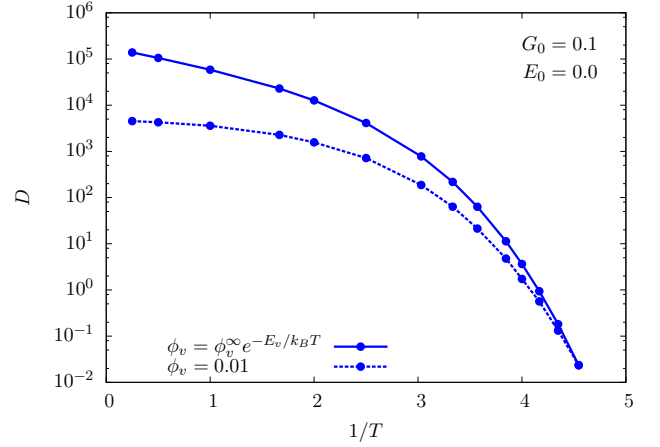


Figure S2. Arrhenius plot of D against $1/T$ at $G_0 = 0.1$ and $E_0 = 0$ for a T -dependent void density $\phi_v(T)$ and a constant $\phi_v = 0.01$.

$\phi_v(T = 0.22) = 0.01$. The result on the diffusion coefficient D is shown in Fig. S2 and is compared with the case with a constant $\phi_v = 0.01$. Using $\phi_v(T)$ from Eq. (S1), D becomes larger at high T due to the increased ϕ_v . By defining T_g at $D_r = 0.1$, Fig. S3 plots D^{-1} against T_g/T . Also shown for comparison are examples of results for other values of G_0 at $\phi_v = 0.01$ from Fig. 2. We observe a spread of the high temperature limiting values of D^{-1} and this removes an artifact introduced by the constant ϕ_v assumption. The fragility, which is predominantly a low T property, on the other hand is much less affected. For $G_0 = 0.1$, the kinetic fragility m_k computed using $\phi_v(T)$ is 19.3. It is slightly higher than the value 16.2 found for the constant $\phi_v = 0.01$ case. Therefore, results on fragility from our simple consideration of a constant ϕ_v are expected to be valid in general.

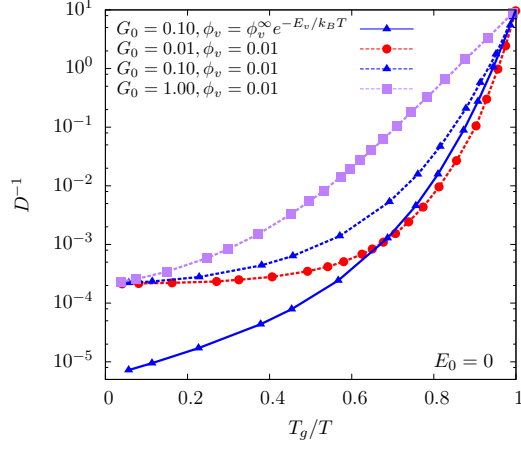


Figure S3. Kinetic Angell plot of D^{-1} against T_g/T for fixed void density $\phi_v = 0.01$ at $G_0 = 0.01, 0.1, 1$ and $E_0 = 0$, with the varying void density case at $G_0 = 0.1$ and $E_0 = 0$. T_g is defined at $D_r = 0.1$.

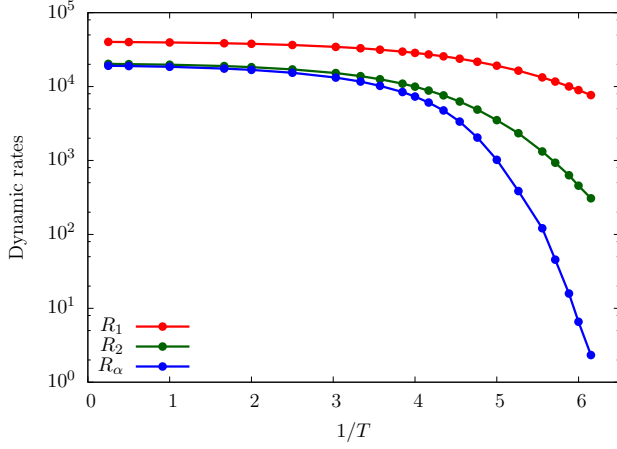


Figure S4. Rate of particle hops R_1 , rate of particle non-returning second hops R_2 , and structural relaxation rate based on mean square displacement R_α against $1/T$ at $G_0 = 0.01$ and $E_0 = 0$.

Hopping rates and return probability: Glassy dynamics has strong temporal correlations characterized by numerous back-and-forth particle hopping motions. We now report analysis on dynamic rates and return probability to study the temporal correlations, following our previous works on polymer simulations [6, 7]. The hopping rate R_1 of any individual particle is defined as the number of hops per particle per unit time. For our fragile glass with $G_0 = 0.01$ and $E_0 = 0$, R_1 is measured from our simulations and results are reported in Fig. S4. For comparison, we have also plotted the structural relaxation rate $R_\alpha = 1/\tau_\alpha$ where the relaxation time τ_α is extracted from the mean square displacement at MSD = 1 (see Fig. S1).

From Fig. S4, we see that R_1 exhibits only a very mild super-Arrhenius slowdown compared with R_α as T

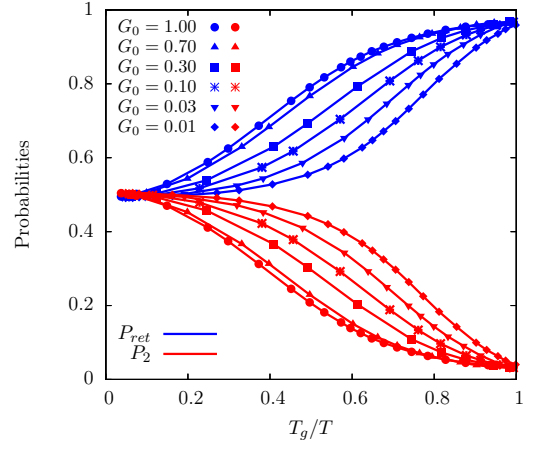


Figure S5. Probabilities of returning hop P_{ret} and non-returning second hop P_2 against T_g/T , with T_g defined at $D = D_r \equiv 0.1$.

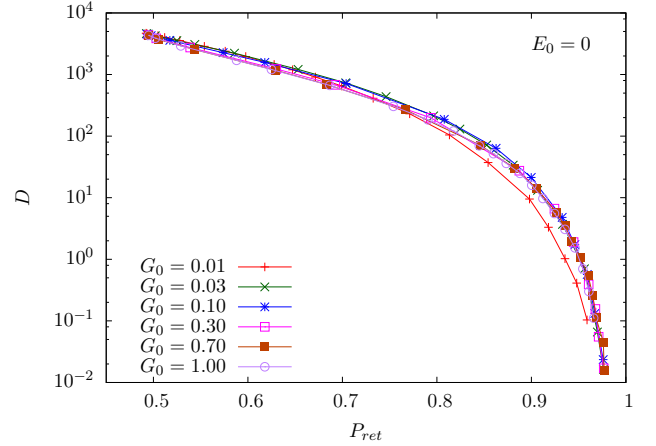


Figure S6. Plot of D against P_{ret} for various G_0 and $E_0 = 0$.

decreases. Assuming isolated voids valid for the small $\phi_v = 0.01$ used, $R_1 = 4\phi_v \langle w \rangle$, where $\langle w \rangle$ is the average of the hopping rate w of a particle next to a void. As defined in Eq. (3), w depends on the hopping energy barrier $E_0 + \Delta E$, where ΔE is the change of the system energy due to the hop. A mild T dependence of R_1 thus implies a mild increase of the relevant hopping barriers as T decreases, which cannot explain the glassy slowdown.

To study hopping correlations, we monitor each particle after its first hop for a long duration. We measure the probability P_{ret} and P_2 that it will next perform either a returning hop to its original position or a second hop to a third position respectively. The rate $R_2 = P_2 R_1$ of a second non-returning hop is also shown in Fig. S4. It is clear that R_2 exhibits a stronger super-Arrhenius T dependence than R_1 . Compared with R_1 , the value of R_2 is closer to R_α and can better characterize the glassy slowdown. Nevertheless, R_2 still shows a slowdown milder than that of R_α . This is because a sequence of two hops

to distinct positions is also often reversed and repeated at low T and may not characterize structural relaxations, as have been observed in polymer simulations [6]. It will be interesting to measure R_n with $n \geq 3$ characterizing the rates of sequences of n non-returning hops after subsequences of back-and-forth hops in between are disregarded. Then, R_n at large n may show the same slowdown as R_α .

Figure S5 plots P_{ret} and P_2 against T_g/T for various values of G_0 . Qualitatively, the result is very similar to that from polymer simulations in [6, 7]. In particular, it supports that $P_{ret} \rightarrow 1$ when $T \rightarrow 0$. P_{ret} has reached 0.97 at the lowest T studied. A high P_{ret} clearly contributes to dynamic slowdown. It signifies highly constrained kinetic pathways resulting from a reduced entropy as argued in the main text. For the most fragile glasses at small G_0 , we observe that P_{ret} rises with T_g/T most abruptly and the rise coincides with the abrupt drop of D . Furthermore, we plot D against P_{ret} for all G_0 at $E_0 = 0$ in Fig. S6, which shows a nice collapse of the data into a single curve. This further supports the strong relevance of P_{ret} to D and thus to m_k . Note that the collapse clearly breaks down for other values of E_0 as only D but not P_{ret} depends on E_0 . The properties of P_2 is complementary to those of P_{ret} since $P_{ret} + P_2 \simeq 1$. The sum $P_{ret} + P_2$ is slightly less than 1 because some particles do not perform a second hop even after a long duration.

Self-intermediate scattering function: Figure S7 shows the self-intermediate scattering function $F_s(\mathbf{q}, t)$ [1] computed from our simulations for the fragile case at $G_0 = 0.01$ and $E_0 = 0$, where $\mathbf{q} = (2\pi/L)\mathbf{q}'$ with $q' = 10$. A very stretched-out relaxation is also observable at low T , analogous to results on the MSD. For example, the relaxation causing $F_s(\mathbf{q}, t)$ to drop from 0.9 to 0.1 covers about three decades in time for the lowest T studied. Compared with results for a strong glass illustrated in Ref. [1], the decay in Fig. S7 for the fragile glass is significantly more stretched out.

Moreover, $F_s(\mathbf{q}, t)$ in Fig. S7 shows apparently a single-step relaxation, which is indeed a two-step relaxation with a tiny first drop only noticeable upon magnification or in a semi-log scale, similar to the case of the strong glass in Ref. [1]. A small first relaxation step is again typical of lattice models due to the lack of vibrations. The main relaxation is well fitted by the Kohlrausch-Williams-Watts (KWW) stretched exponential function $A \exp(-(t/\tau)^\beta)$ at sufficiently large t beyond the first relaxation step. Here, β is the stretching exponent while τ and $A \simeq 1$ are the relaxation time and the decay magnitude of the main relaxation. Specifically, we extract β from the fit around $F_s(\mathbf{q}, t) = 1/e$. For other values of G_0 , values of β are similarly obtained.

Results for $E_0 > 0$ can be obtained from those for $E_0 = 0$ after performing a rescaling of time as explained above for the calculations of D . While the time rescaling alters $F_s(\mathbf{q}, t)$, it does not affect β for any fixed T . Therefore, the value of β at T_g depends on E_0 only via T_g . Figure S8

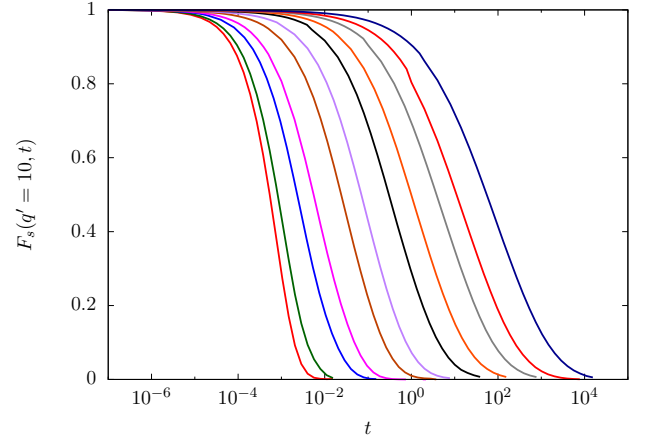


Figure S7. $F_s(\mathbf{q}, t)$ against t at $G_0 = 0.01$ and $E_0 = 0$ with $q' = 10$. Different curves represent different temperatures at $T = 0.4, 0.3, 0.24, 0.22, 0.2, 0.19, 0.18, 0.175, 0.17, 0.1667, 0.1626$ (from left to right).

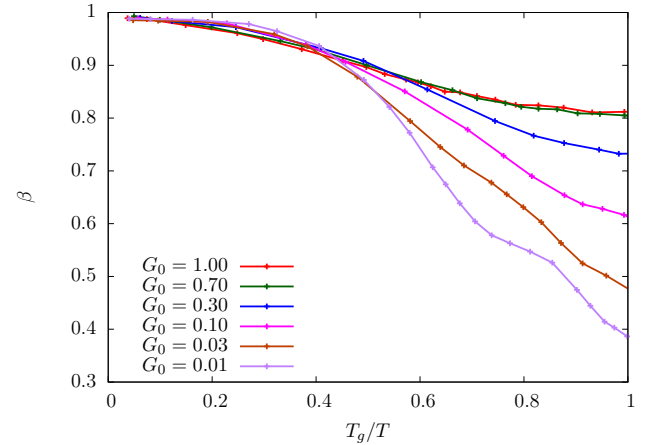


Figure S8. β against T_g/T at $G_0 = 0.01, 0.03, 0.1, 0.3, 0.7, 1$. T_g is extracted at $D_r = 0.1$ for $E_0 = 0$.

shows the plot of β against T_g/T for all values of G_0 at $E_0 = 0$. Using these and similar results for $E_0 > 0$, we perform third-order polynomial fits to the dependence of β on T_g/T to provide the best estimate of β at T_g , which are used in Fig. 3 in the main text.

We have also computed the structural relaxation time τ defined using the self-intermediate scattering function by $F_s(q' = 10, t = \tau) = e^{-1}$. The corresponding Arrhenius plot and kinetic Angell plot are shown in Figs. S9 and S10, where T_g in Fig. S10 is defined as T at which $\tau = 100$. Qualitatively, results in Figs. S10 and 2 are fully analogous. Quantitatively, at low T , τ diverges faster than D^{-1} , leading to the Stoke-Einstein violation shown in Fig. S11. It is clear from Fig. S11 that the fragile systems exhibit a stronger violation.

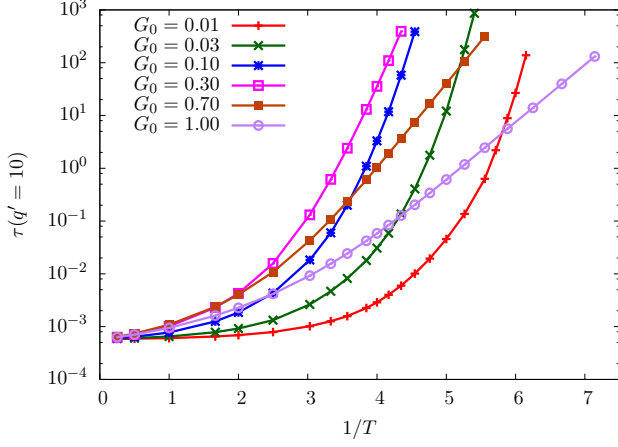


Figure S9. Arrhenius plot of τ for various G_0 at $E_0 = 0$.

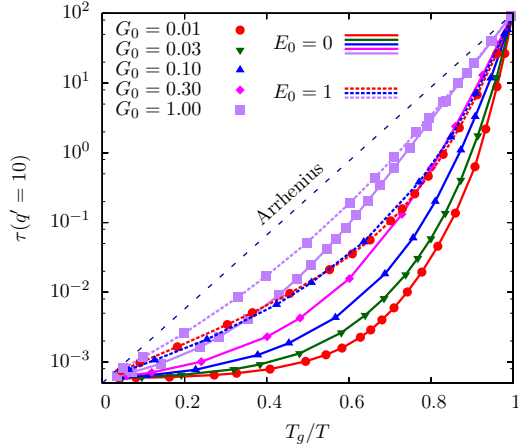


Figure S10. Kinetic Angell plot of τ against T_g/T for various G_0 and E_0 , where T_g for each curve is defined at $\tau_r = 100$.

Kinetic and thermodynamic fragilities: We have calculated the kinetic and thermodynamic fragilities m_k and m_t for various values of G_0 and E_0 . Results are shown in Figs. S12 and S13 respectively. We observe empirically that for $G_0 \lesssim 0.7$, both m_k and m_t decrease linearly with $\log G_0$. Furthermore, m_k increases significantly as E_0 decreases for small G_0 . Otherwise, for m_t and m_k at large G_0 , the dependence on E_0 is weak. Combining the results in Figs. S12 and S13, we obtain the plot of m_t against m_k in Fig. 4 in the main text.

III. KINETIC FRAGILITY EXTRAPOLATED TO REALISTIC TIME SCALE

Experimental values of the kinetic fragility m_k range typically from about 25 to 150 [8]. Our simulations give values from 6.76 to 26.35 which are in contrast a few times smaller. Nevertheless, this is only because we have adopted a large reference diffusion coefficient $D_r = 0.1$ in

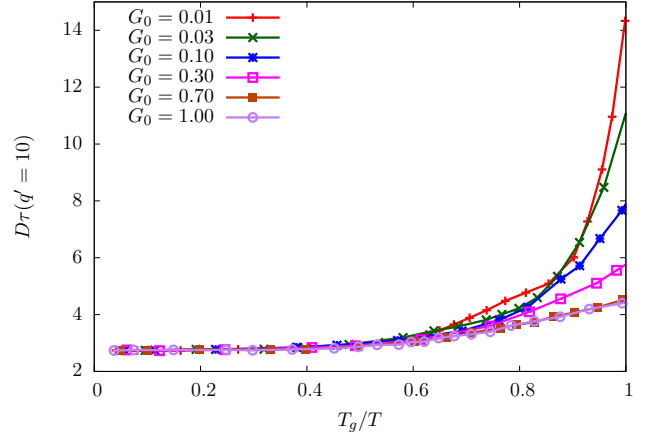


Figure S11. Plot of $D\tau$ against T_g/T for various G_0 , with τ evaluated at $q' = 10$ and T_g defined at $D_r = 0.1$. The non-constancy of $D\tau$ with respect to T indicates the violation of the Stoke-Einstein relation.

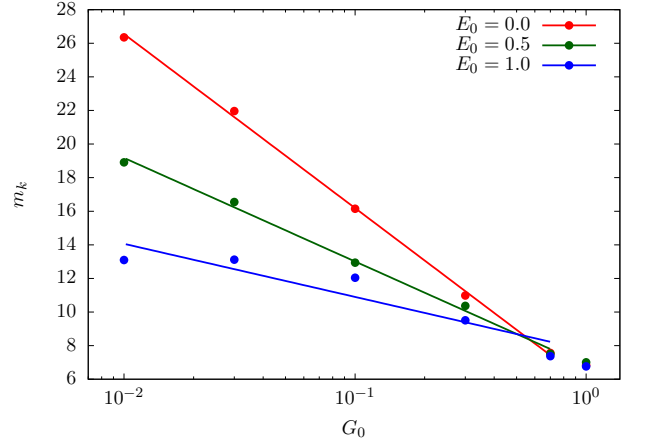


Figure S12. m_k against G_0 at $E_0 = 0, 0.5, 1$. m_k is computed at $D_r = 0.1$.

the definition of T_g because of computational limitations. In fact, similar to all microscopic particle simulations, our DPLM simulations correspond to very short physical time scales compared with experimental situations. Adopting a much smaller D_r in direct analysis of simulations is not feasible because the required simulations would involve much slower dynamics. Here, we show that by extrapolating to a realistic value of D_r , corresponding to a much longer time scale, the obtained values of m_k increase significantly and are consistent with the typical experimental range.

We compute

$$m_k = \left. \frac{\partial \log D^{-1}}{\partial (T_g/T)} \right|_{T=T_g} \quad (\text{S2})$$

numerically from the values of D close to T_g . We define T_g as the temperature at which $D = D_r$ with $D_r = 0.1$.

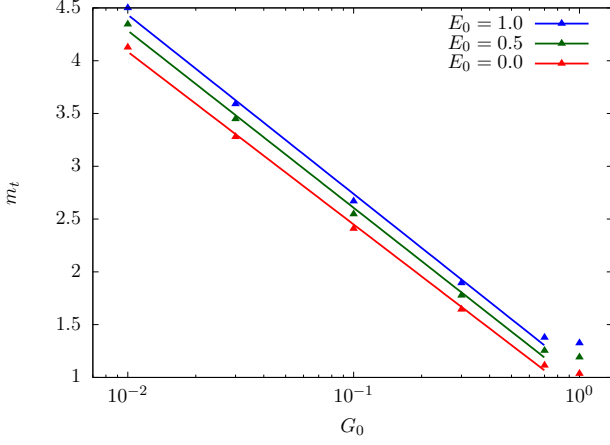


Figure S13. m_t against G_0 at $E_0 = 0, 0.5, 1$. m_t is computed at T_g at which $D_r = 0.1$.

Let us first consider the strong glass limit corresponding to Arrhenius dynamics with the smallest possible kinetic fragility m_k^{strong} . As $T \rightarrow \infty$, the model reduces to a simple lattice gas. The diffusion coefficient is approximately given by

$$D_\infty \simeq \frac{(z-2)w_0\phi_v}{2d} \quad (S3)$$

with the coordination number $z = 2d$ and dimension $d = 2$ [9]. It evaluates to $D_\infty \simeq 5 \times 10^3$ for small $\phi_v = 0.01$. Assuming an Arrhenius T dependence of D , Eq. (S2) gives $m_k^{strong} = \log(D_\infty/D_r) \simeq 4.70$. This is close to $m_k = 6.76$ for the strongest glass we have considered at $G_0 = 1$ and $E_0 = 1$ in the main text. We next consider a more realistic value of $D_r = 10^{-14}$. This value is chosen so that as T varies from T_g to ∞ , D varies by nearly 18 orders of magnitude, a variation comparable to typical experimental ranges [10, 11]. This gives $m_k^{strong} = 21.4$, which is consistent with experimental values for strong glasses.

For the case of fragile glasses, we have obtained a large kinetic fragility $m_k^{fragile} = 26.35$ at $G_0 = 0.01$ and $E_0 = 0$ based on $D_r = 0.1$. More generally, Fig. S14 plots $m_k^{fragile}$ obtained from simulations for $D_r = 0.2, 0.1414, 0.1, 0.707$ and 0.05 . For $D_r < 0.1$, we have performed a parabolic extrapolation to data in Fig. 1 and computed $m_k^{fragile}$ using Eq. (S2) based on the extrapolated values of D . The result shows an empirical relation $m_k^{fragile} \sim \ln D_r$. An extrapolation using this relation to $D_r = 10^{-14}$, we get $m_k^{fragile} = 120$, which is more consistent with the experimental range. In principle, by extrapolating our simulation results towards $G_0 \rightarrow 0$, the kinetic fragility m_k appears to rise unboundedly.

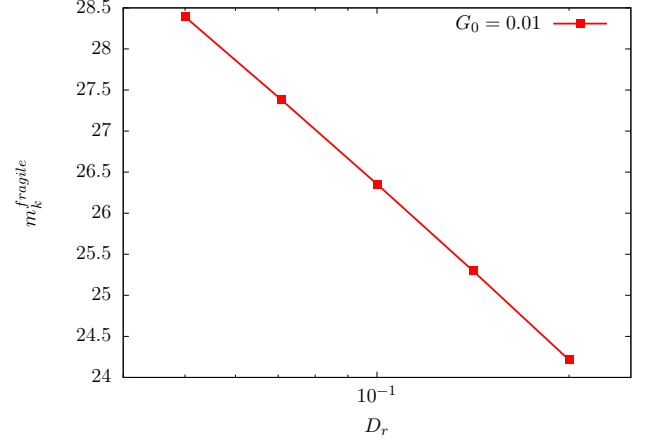


Figure S14. Kinetic fragility $m_k^{fragile}$ against D_r for $G_0 = 0.01$ and $E_0 = 0$.

IV. EXACT EQUILIBRIUM STATISTICS AND NUMERICAL VERIFICATIONS

We first summarize the equilibrium statistics of the DPLM on the 2D square lattice developed in [1]. Simulations are all performed in an canonical ensemble with a set of N particles. The partition function in canonical ensemble is given by

$$Z = \sum_{\{s_i\}} e^{-E/k_B T}, \quad (S4)$$

where the sum is over all possible particle configurations $\{s_i\}$ and E is the system energy given in Eq. (1). Here, s_i denotes the particle at site i , with $s_i = 0$ denoting instead a void. The occupation state at site i can be expressed as $n_i = 1 - \delta_{s_i,0}$, where δ is the Kronecker delta. Equation (S4) can be rewritten as a sum over different occupation states as

$$Z = \sum_{\{n_i\}} Z_{\{n_i\}}, \quad (S5)$$

where the partition function for a given occupation state $\{n_i\}$ is given by

$$Z_{\{n_i\}} = \sum_{\{s_i > 0\} \in \mathcal{P}_N} \prod_{<i,j>} e^{-V_{s_i s_j}/k_B T}. \quad (S6)$$

after using Eq. (1). Here, \mathcal{P}_N denotes the set of all permutations of the N particles and the product is over all nearest neighboring sites i and j .

At the thermodynamic (i.e. large N) limit, it was shown in [1] that an average over particle permutations \mathcal{P}_N gives exactly

$$\frac{Z_{\{n_i\}}}{N!} = e^{-N_b U/k_B T}, \quad (S7)$$

where N_b is the number of nearest neighboring particle bonds in the system and U is the free energy of the corresponding interactions defined by

$$U = -k_B T \ln \int e^{-V/k_B T} g(V) dV. \quad (\text{S8})$$

Applying Eqs. (S5) and (S7), the exact partition function can be written as

$$Z = N! \sum_{\{n_i\}} e^{-N_b U/k_B T}. \quad (\text{S9})$$

Note that no ensemble averaging over the interactions V_{kl} has been performed yet, but they are already averaged out by the particle permutation averaging. Therefore, both quenched and annealed ensemble averaging over the interactions trivially arrive at the same exact partition function Z in Eq. (S9).

Using Eqs. (S5) and (S6) and the applicability of annealed averaging, it was shown in [1] that a realized interaction $V_{s_i s_j}$ follows exactly the Boltzmann distribution

$$p_{eq}(V) = \frac{1}{\mathcal{N}} e^{-V/k_B T} g(V) \quad (\text{S10})$$

where

$$\mathcal{N} = \int e^{-V/k_B T} g(V) dV \quad (\text{S11})$$

is a normalization constant. The system energy E in Eq. (1) then gives

$$E = N_b^* \bar{V} \quad (\text{S12})$$

where N_b^* is the most probable value of the number of interactions in the system and \bar{V} is the average realized interaction energy given by

$$\bar{V} = \int V p_{eq}(V) dV. \quad (\text{S13})$$

The availability of an exact partition function Z in Eq. (S9) and the resulting exact equilibrium properties are remarkable properties of the DPLM. It is in our knowledge unique among energetically non-trivial models of glass defined on the square lattice and it has no counterpart for the closely related problem of spin glass. This highly surprising feature requires careful scrutiny. The exact distribution $p_{eq}(V)$ in Eq. (S10) can be verified to a high precision by histograms of realized interactions in equilibrated systems. Examples of results are reported in [1] and [12]. The verification of the exact energy E in Eq. (S12) will also be explained later. Note that the validity of the exact expressions of $p_{eq}(V)$ and E in Eqs. (S10) and (S12) rely directly on the validity of the exact partition function Z in Eq. (S9).

From Eq. (S9), it is clear that DPLM shares the same equilibrium particle occupation statistics with a simple lattice gas model with a uniform nearest neighboring particle interaction energy U . On the 2D square

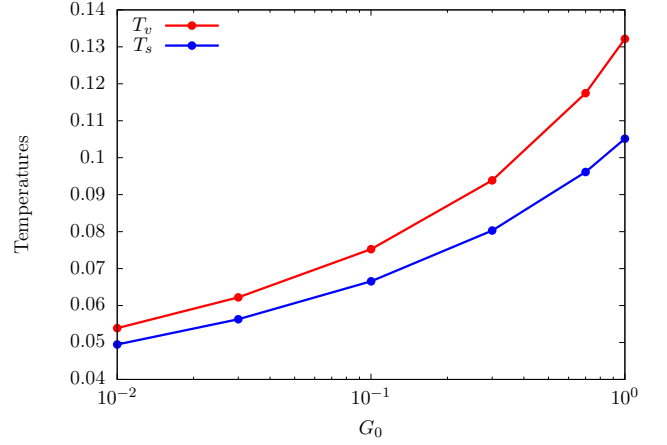


Figure S15. Vaporization temperature T_v and phase separation temperature T_s against G_0 , where T_s is evaluated at a void density $\phi_v = 0.01$.

lattice, the simple lattice gas model admits a particle condensation-evaporation transition corresponding to the ferromagnetic-paramagnetic transition of the Ising model with an exchange interaction $J = -U/4$ [13]. It occurs at a vaporization temperature T_v , given exactly by the Onsager solution [14]

$$T_v = \frac{-U}{2 \ln(1 + \sqrt{2})}. \quad (\text{S14})$$

For $G_0 = 1$, we get $T_v = 0.132$ as evaluated in [1]. Figure S15 plots T_v for all values of G_0 .

The condensation-evaporation transition at T_v is readily observable in the DPLM. We have observed from real-space animations at $G_0 = 1$ and $\phi_v = 0.5$ typical spinodal decomposition into co-existing particle and void aggregates as T is decreased below T_v . Theoretically, the exact partition function Z in Eq. (S9) remains valid both below and above T_v for the DPLM, analogous to the case of a simple lattice gas. The transition manifests itself through the non-analyticity of N_b^* and thus also of E at T_v [14].

In all simulations reported in this work, we consider T well above T_v so that no macroscopic void cluster exists. This is because in the evaporation phase, particle and void aggregates are miscible and two-phase co-existence is not applicable. It represents the physical regime we are interested in since large void aggregates do not typically exist in equilibrated supercooled liquids with few free volumes. Furthermore, large void aggregates in fact is not guaranteed to form even below T_v due to the small void density ϕ_v . Below T_v , the occurrence of macroscopic aggregates of the minority component, i.e. the voids, is further controlled by the phase separation temperature $T_s \leq T_v$. Only for $T < T_s$, macroscopic particle condensates and void clusters become immiscible and phase separates. Here, T_s is obtained by solving the Onsager-Yang equation [15, 16]. For the DPLM, it is given exactly

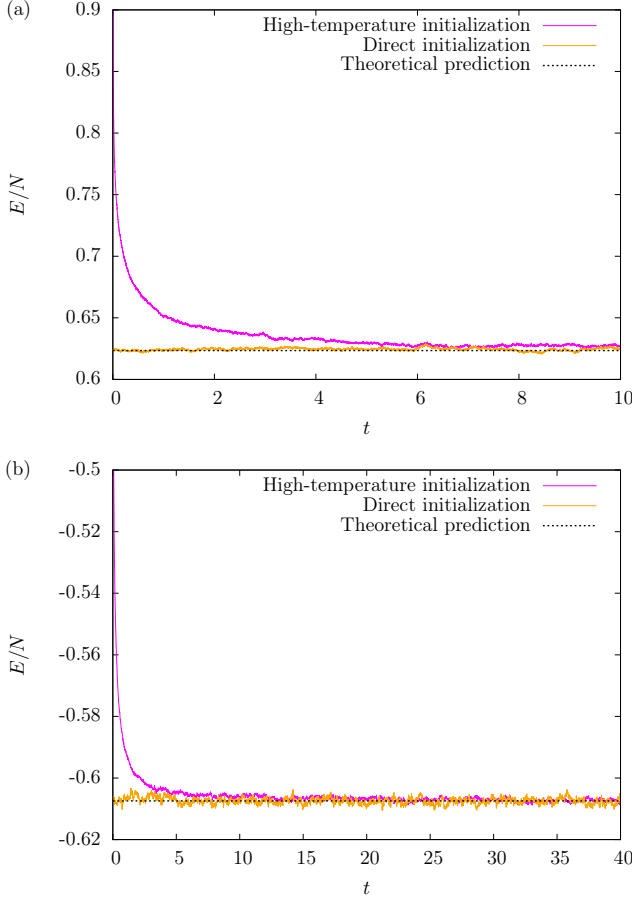


Figure S16. Plots of energy per particle E/N against time t from simulations at $T = 0.2$ and $\phi_v = 0.01$ using a high-temperature initialization (purple line) and a direct initialization method (orange line). The black dotted lines show theoretical predictions of the equilibrium values using Eq. (S18). We take $G_0 = 0.01$ (a) and 1 (b).

by

$$T_s = \frac{-U}{2 \sinh^{-1} \left[(1 - (2\phi_v - 1)^8)^{-\frac{1}{4}} \right]}. \quad (\text{S15})$$

For $\phi_v = 0.01$, the results on T_s for different G_0 is also plotted in Fig. S15.

At a first sight, the possible occurrence of phase separation at T_v in addition to the glass transition at T_g appears to complicate the description of glass by the DPLM. However, this is not the case. From Eq. (S15), as $\phi_v \rightarrow 0$, $T_s \rightarrow 0$, meaning that macroscopic void aggregates can be avoided at arbitrarily low T by selecting a sufficiently small ϕ_v . There thus exists the physically relevant situation with an increasingly small void density ϕ_v as T decreases (see e.g. Eq. (S1)) so that T_s is always below T . Thus, phase separation should not occur and no macroscopic void aggregate appears at any T .

Results above are exact for arbitrary ϕ_v . Now, we assume a small ϕ_v so that voids are mostly isolated. This is

justified for all simulations reported in this work because $T \gg T_s$ with T_s shown in Fig. S15. Voids clusters must be so small that voids are isolated most of the time as is observable through the real-space visualizations (see Fig. 7 and videos in [1]). Assuming isolated voids, the number of particle interactions in the system follows

$$N_b = 2N(1 - \phi_v), \quad (\text{S16})$$

which is now a constant independent of the occupation state $\{n_i\}$. Using Eq. (S9), the partition function after summing over the occupation states is

$$Z = N! \mathcal{M} e^{-\beta N_b U}, \quad (\text{S17})$$

where \mathcal{M} is the number of possible particle occupation states. On the other hand, Eq. (S12) becomes

$$\frac{E}{N} = 2(1 - \phi_v) \bar{V}, \quad (\text{S18})$$

noting that $N_b^* = N_b$. The exact system energy E from Eq. (S18) is another non-trivial result following from the exact equilibrium statistics and the isolated void assumption. To verify its validity, Fig. S16 plots examples of the time-evolution of E/N for systems randomly initialized at $T = \infty$. It converges well to the exact value from Eq. (S18). This verifies Eq. (S18) which in turn verifies both the exact equilibrium statistics and the isolated void assumption.

In our main simulations, we apply a direct initialization method introduced in [1]. Specifically, a simple lattice gas with interaction U is first equilibrated, which is a very rapid procedure even at low T . Unrealized interactions V_{kl} are then sampled based on the *a priori* distribution $g(V)$ while the realized interactions $V_{s_i s_j}$ are instead sampled from the *a posteriori* distribution $p_{eq}(V)$ given in Eq. (S10). The system energy E , also shown in Fig. S16, is already stable right after the sampling. This verifies the validity of the direct initialization method and hence again of the exact equilibrium statistics from which the method is derived.

V. ENTROPY AT SMALL VOID DENSITY

For small ϕ_v , using the partition function Z given in Eq. (S17), the system entropy S can be calculated straight-forwardly. From simple combinatorics, $\mathcal{M} = C(L^2, N_v)$, where $N_v = L^2 \phi_v \simeq N \phi_v$ denotes the number of voids. Using $\ln n! \simeq n \ln n - n$, we get

$$\ln \mathcal{M} = N_v (\ln(L^2/N_v) + 1) = N_v (1 - \ln \phi_v). \quad (\text{S19})$$

Using Eqs. (S17) and (S19), the Helmholtz free energy $F = -k_B T \ln Z$ equals

$$F = N_b U - k_B T N_v (1 - \ln \phi_v) - k_B T N (\ln N - 1). \quad (\text{S20})$$

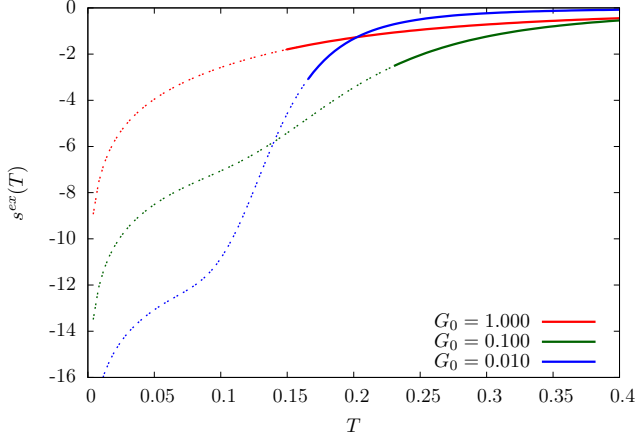


Figure S17. Equilibrium excess entropy per particle s^{ex} against T at various G_0 for $T > T_g$ (solid lines) and $T < T_g$ (dotted lines). Note that results are of directly experimental relevance only for $T > T_g$, as equilibrium systems are in general available experimentally only under this condition.

From the thermodynamic relation $F = E - TS$ with $E = N_b \bar{V}$, we get

$$S = \frac{N_b (\bar{V} - U)}{T} + N k_B \phi_v (1 - \ln \phi_v) + N k_B (\ln N - 1), \quad (\text{S21})$$

Defining the entropy per particle as $s = S/N$, we further define an excess entropy per particle $s^{ex}(T) = s(T) - s^{LG}$ relative to the entropy $s^{LG} = k_B \phi_v (1 - \ln \phi_v) + k_B (\ln N - 1)$ of a simple lattice gas [17]. Equations (S16) and (S21) then give

$$s^{ex} = \frac{2(1 - \phi_v)(\bar{V} - U)}{T} \quad (\text{S22})$$

Applying Eqs. (2), (S8), (S10) and (S13) and after some straight-forward algebra, we get

$$s^{ex} = 2k_B(1 - \phi_v) \left\{ 1 + \ln \left[(G_0/\Delta V) k_B T (1 - e^{-\Delta V/k_B T}) + (1 - G_0) e^{-\Delta V/k_B T} \right] + \frac{[(1 - G_0)\Delta V/k_B T - 1]}{(G_0/\Delta V) k_B T (e^{\Delta V/k_B T} - 1) + (1 - G_0)} \right\}, \quad (\text{S23})$$

which is exact at the small ϕ_v limit. Figure S17 shows the result for s^{ex} at $G_0 = 0.001, 0.01, 0.1$, and 1 . As T decreases, a significant drop of s^{ex} occurs around $T \simeq 0.15$ and it becomes more and more dramatic as G_0 decreases.

This dramatic and controllable drop of s^{ex} around $T \simeq 0.15$ is the main cause of the high fragilities at small G_0 . It results from a shift of the relative importance of the two components in $g(V)$. It can be intuitively understood by studying the interplay between the two components as follows. The bicomponent $g(V)$ in Eq. (2) in the main text can be written as

$$g(V) = g_A(V) + g_B(V) \quad (\text{S24})$$

where components labeled A and B are the uniform and Dirac distributions given by

$$g_A(V) = \frac{G_0}{\Delta V}, \quad (\text{S25})$$

$$g_B(V) = (1 - G_0)\delta(V - V_1). \quad (\text{S26})$$

for $V \in [V_0, V_1]$ with $\Delta V = V_1 - V_0$. Generalizing Eqs. (S11), (S13), (S8) and (S22) to individual components, we write

$$\mathcal{N}_{A,B} = \int e^{-V/k_B T} g_{A,B}(V) dV, \quad (\text{S27})$$

$$\bar{V}_{A,B} = \frac{1}{\mathcal{N}_{A,B}} \int V e^{-V/k_B T} g_{A,B}(V) dV, \quad (\text{S28})$$

$$U_{A,B} = -k_B T \ln \int e^{-V/k_B T} g_{A,B}(V) dV, \quad (\text{S29})$$

$$s_{A,B}^{ex} = \frac{2(1 - \phi_v)(\bar{V}_{A,B} - U_{A,B})}{T}. \quad (\text{S30})$$

which satisfy $\mathcal{N} = \mathcal{N}_A + \mathcal{N}_B$. These equations evaluate to

$$\mathcal{N}_A = \frac{G_0 k_B T}{\Delta V} e^{-V_0/k_B T} (1 - e^{-\Delta V/k_B T}), \quad (\text{S31})$$

$$\bar{V}_A = V_0 + k_B T - \frac{\Delta V}{e^{\Delta V/k_B T} - 1}, \quad (\text{S32})$$

$$U_A = V_0 - k_B T \ln \left[\frac{G_0 k_B T}{\Delta V} (1 - e^{-\Delta V/k_B T}) \right], \quad (\text{S33})$$

$$s_A^{ex} = 2k_B(1 - \phi_v) \left\{ 1 + \ln \left[\frac{G_0 k_B T}{\Delta V} (1 - e^{-\Delta V/k_B T}) \right] - \frac{\Delta V}{k_B T} \frac{1}{e^{\Delta V/k_B T} - 1} \right\}, \quad (\text{S34})$$

and

$$\mathcal{N}_B = (1 - G_0) e^{-(V_0 + \Delta V)/k_B T}, \quad (\text{S35})$$

$$\bar{V}_B = V_0 + \Delta V, \quad (\text{S36})$$

$$U_B = V_0 + \Delta V - k_B T \ln(1 - G_0), \quad (\text{S37})$$

$$s_B^{ex} = 2k_B(1 - \phi_v) \ln(1 - G_0). \quad (\text{S38})$$

Then, s^{ex} can alternatively be calculated using the standard expression for two-state systems:

$$s^{ex} = X s_A^{ex} + (1 - X) s_B^{ex} - X k_B \ln X - (1 - X) k_B \ln(1 - X), \quad (\text{S39})$$

where $X = \mathcal{N}_A/\mathcal{N} = \mathcal{N}_A/(\mathcal{N}_A + \mathcal{N}_B)$ is the probabilistic weight of component A . Equation (S39) also evaluates to Eq. (S23) after some algebra. In Eq. (S39), the first two terms are the contributions of the two components alone. The remaining terms are the entropy due to the mixing of the components, which approaches 0 for X approaching 0 or 1.

Consider $G_0 \ll 1$ corresponding to the regime relevant to fragile glasses. Eqs. (S31) and (S35) gives

$$\frac{\mathcal{N}_A}{\mathcal{N}_B} = \frac{G_0 k_B T}{\Delta V} e^{\Delta V/k_B T} (1 - e^{-\Delta V/k_B T}). \quad (\text{S40})$$

Then

$$\frac{\mathcal{N}_A}{\mathcal{N}_B} = \begin{cases} 0 & \text{for } T \rightarrow \infty \\ \infty & \text{for } T \rightarrow 0 \end{cases} \quad (\text{S41})$$

and hence

$$X = \begin{cases} 0 & \text{for } T \rightarrow \infty \\ 1 & \text{for } T \rightarrow 0. \end{cases} \quad (\text{S42})$$

Physically, component A corresponds to the low energy states important at low T while component B corresponds to the numerous states important at high T . Equation (S39) then implies

$$s^{ex} = \begin{cases} s_B^{ex}(T \rightarrow \infty) = 0 & \text{for } T \rightarrow \infty \\ s_A^{ex}(T \rightarrow 0) & \text{for } T \rightarrow 0 \end{cases} \quad (\text{S43})$$

where Eq. (S38) is also used. At $T \rightarrow 0$, Eq. (S34) simplifies to

$$s_A^{ex}(T \rightarrow 0) = 2k_B(1 - \phi_v) \left[1 + \ln \left(\frac{G_0 k_B T}{\Delta V} \right) \right], \quad (\text{S44})$$

and we have considered $k_B T \ll \Delta V$ for simplicity. At small G_0 and low T , due to the $\ln G_0$ dependence, $s_A^{ex}(T \rightarrow 0)$ is small and hence s^{ex} is also small. This explains the dramatic drop of s^{ex} from 0 as T decreases at small G_0 .

VI. BICOMPONENT INTERACTION DISTRIBUTION AND BOND EXCITATION MODEL

Note that the bicomponent $g(V)$ in Eq. (2) is fully analogous to a bond excitation model, also called the two-state model, of glass proposed in Ref. [18], which considers microscopic states suggested as particle bonds taking either a low-entropy unexcited state or a high-entropy excited state. Although our component A is a band of

states, the energy spread becomes narrow at low T and this contributes to the similarity between the models. In Ref. [18], the entropy difference ΔS^0 and the enthalpy difference ΔH^0 between excited and unexcited state are the fitting parameters for the entropy for different materials. In our model, we can calculate ΔS^0 and ΔH^0 as follows. By dividing Eqs. (S34) and (S38) by $2(1 - \phi_v)$, we get the entropy per bond for the unexcited and excited state respectively. The entropy difference ΔS^0 is then $\Delta S^0 = (s_B^{ex} - s_A^{ex})/[2(1 - \phi_v)]$, which gives

$$\Delta S^0 = k_B \left\{ \ln \left[\frac{(1 - G_0)}{G_0(1 - e^{-\Delta V/k_B T})} \frac{\Delta V}{k_B T} \right] + \frac{\Delta V}{k_B T} \frac{1}{e^{\Delta V/k_B T} - 1} - 1 \right\}. \quad (\text{S45})$$

On the other hand, ΔH^0 is simply given by $\Delta H^0 = \bar{V}_B - \bar{V}_A$. Using Eqs. (S32) and (S36),

$$\Delta H^0 = k_B T \left[\frac{\Delta V}{k_B T} \left(1 + \frac{1}{e^{\Delta V/k_B T} - 1} \right) - 1 \right]. \quad (\text{S46})$$

For the fragile glass with $G_0 = 0.01$ and $E_0 = 0$, our DPLM simulations give $T_g \simeq 0.163$. Noting that $k_B = \Delta V = 1$, Eqs. (S45) and (S46) give $\Delta S^0/k_B = 5.42$ and $\Delta H^0/k_B T_g = 5.15$ at $T = T_g$. This can be compared with the fragile glass of toluene for example. By fitting to experimental results on entropy measurements, the bond excitation model gives $\Delta S^0 = 45.4$ J/mol·K and $\Delta H^0 = 6760$ J/mol, expressed in terms of per mole of excitable states [18]. Taking $k_B = 8.315$ J/mol·K and $T_g = 117$ K, they lead to $\Delta S^0/k_B = 5.46$ and $\Delta H^0/k_B T_g = 6.95$. Toluene is considered because this value of $\Delta S^0/k_B$ matches the value 5.42 from DPLM simulations. The consistency of the value of $\Delta H^0/k_B T_g = 6.95$ with the DPLM result of 5.15 then provides an additional support of the close relation between the bond excitation model and the DPLM with the bicomponent form of $g(V)$.

-
- [1] L.-H. Zhang and C.-H. Lam, “Emergent facilitation behavior in a distinguishable-particle lattice model of glass,” *Phys. Rev. B* **95**, 184202 (2017).
 - [2] T. Damart and D. Rodney, “Atomistic study of two-level systems in amorphous silica,” *Phys. Rev. B* (2018), 10.1103/PhysRevB.97.014201.
 - [3] W. Kob and H. C. Andersen, “Kinetic lattice-gas model of cage effects in high-density liquids and a test of mode-coupling theory of the ideal-glass transition,” *Phys. Rev. E* **48**, 4364 (1993).
 - [4] H.-Y. Deng, C.-S. Lee, M. Lulli, L.-H. Zhang, and C.-H. Lam, “Configuration-tree theoretical calculation of the mean-squared displacement of particles in glass formers,” *J. Stat. Mech.* **2019**, 094014 (2019).
 - [5] C. Y. Liao and S-H Chen, “Dynamics of inherent structure in supercooled liquids near kinetic glass transition,” *Phys. Rev. E* **64**, 031202 (2001).
 - [6] C.-H. Lam, “Repetition and pair-interaction of string-like hopping motions in glassy polymers,” *J. Chem. Phys.* **146**, 244906 (2017).
 - [7] C.-H. Lam, “Deeper penetration of surface effects on particle mobility than on hopping rate in glassy polymer films,” *J. Chem. Phys.* **149**, 164909 (2018).
 - [8] M. Matthieu, “Relaxation and physical aging in network glasses: a review,” *Rep. Prog. Phys.* **79**, 066504 (2016).
 - [9] C.-H. Lam, “Local random configuration-tree theory for string repetition and facilitated dynamics of glass,” *J. Stat. Mech.* **2018**, 023301 (2018).
 - [10] C. A. Angell, “Relaxation in liquids, polymers and plastic crystals — strong/fragile patterns and problems,” *J. Non-Cryst. Solids* **131-133**, 13 (1991).
 - [11] C. Alba, L. E. Busse, D. J. List, and C. A. Angell,

- “Thermodynamic aspects of the vitrification of toluene, and xylene isomers, and the fragility of liquid hydrocarbons,” *J. Chem. Phys.* **92**, 617 (1990).
- [12] M. Lulli, C. S. Lee, H. Y. Deng, C. T. Yip, and C. H. Lam, “Spatial Heterogeneities in Structural Temperature Cause Kovacs’ Expansion Gap Paradox in Aging of Glasses,” *Phys. Rev. Lett.* (2020), 10.1103/PhysRevLett.124.095501.
- [13] Andreas Nußbaumer, Johannes Zierenberg, Elmar Bittner, and Wolfhard Janke, “Numerical test of finite-size scaling predictions for the droplet condensation-evaporation transition,” *Journal of Physics: Conference Series* **759**, 012009 (2016).
- [14] M. Toda, R. Kubo, and N. Saito, *Statistical physics I: equilibrium statistical mechanics* (Springer, Heidelberg, 1991).
- [15] L. Onsager, “Statistical hydrodynamics,” *Il Nuovo Cimento Series 9* (1949), 10.1007/BF02780991.
- [16] C. N. Yang, “The spontaneous magnetization of a two-dimensional ising model,” *Phys. Rev.* **85**, 808 (1952).
- [17] J. C. Dyre, “Perspective: Excess-entropy scaling,” *J. Chem. Phys.* **149**, 210901 (2018).
- [18] C. T. Moynihan and C. A. Angell, “Bond lattice or excitation model analysis of the configurational entropy of molecular liquids,” *J. Non-Cryst. Solids* **274**, 131 (2000).